Available online at www.sciencedirect.com
ScienceDirect
Journal of the European Ceramic Society 28 (2008) 1235–1242
www.elsevier.com/locate/jeurceramsoc

Dynamic hardness and elastic modulus calculation of porous SiAlON ceramics using depth-sensing indentation technique

Osman Sahin [a,*], Orhan Uzun [b], Małgorzata Sopicka-Lizer [c], Hasan Gocmez [d], Uğur Kölemen [b]

[a] *Suleyman Demirel University, Department of Physics, Isparta, Turkey*
[b] *Gaziosmanpaşa University, Department of Physics, Tokat, Turkey*
[c] *Silesian University of Technology, Department of Materials Science, Katowice, Poland*
[d] *Department of Ceramic Engineering, Dumlupinar University, Kutahya, Turkey*

Received 18 April 2007; received in revised form 5 September 2007; accepted 15 September 2007
Available online 19 November 2007

Abstract

Interest in characterizing the mechanical properties of porous materials at micro-/nanometer scales has increased due to recent development of micro-/nanosystems. Depth-sensing indentation (DSI) systems, also referred to as nanoindentation, are strong tools for performing indentation measurements. The load-displacement curves of SiAlON-based porous ceramics were measured under different peak load (200–1800 mN). The most commonly used Oliver–Pharr method was used to analyze the unloading segments of these curves. The experimental results revealed that the dynamic hardness (H_d) and reduced elastic modulus (E_r) exhibit peak-load dependence, i.e., indentation size effect (ISE). Such peak-load dependence requires calculation of the load-independent hardness (H_{LI}) and elastic modulus (E_r). The experimental hardness data were analyzed using Meyer's law, Hays–Kendall's model, the proportional specimen resistance (PSR) model, and the modified PSR (MPSR) model. As a result, the modified PSR model is found to be the most effective one for H_d determination of these SiAlON ceramics.

Keywords: Mechanical properties; Hardness; SiAlON; Depth-sensing indentation technique; Indentation

1. Introduction

Silicon nitride-based materials or SiAlON ceramics are widely used in high-temperature applications due to their excellent mechanical, physical, and chemical properties.[1] However, because of the covalent bond character, oxide sintering aids or a suitable mixture of oxides and nitrides are commonly used for densification via a transient liquid phase; application of nitrogen overpressure or hot pressing technique is often necessary.[2–4] Because of the deterioration of the glassy phase at elevated temperature, several methods were developed for the production of silicon nitride-based or SiAlON ceramics either without any additives or with additives which are subjected to evaporation during/after densification.[5–8] On the other hand, the absence of the grain boundary liquid phase during sintering contributes to the formation of porous ceramics. Such porous silicon nitride-based or SiAlON ceramics are of great technological interest because of their excellent corrosion resistance both at room and elevated temperatures.[9] They can be applied as ceramic bulk filters in new power-generation systems, e.g. pressurized fluidized bed combustion or integrated coal gasification combined cycle.[10] To date, little has been reported on the mechanical properties of β-SiAlON-based porous ceramics; the hardness evaluation of these porous ceramics is challenging.

Indentation hardness as a principal parameter for the mechanical characterization of materials has been commonly used as a technique to measure the mechanical properties of materials. Two methods of Vickers microindentation hardness measurement are practically in use. In one method, a hard indenter (i.e., a Vickers diamond pyramid) penetrates into the solid with a constant load. After unloading, the dimensions of the indentation in the solid are measured and the hardness, defined as the ratio of

* Corresponding author. Tel.: +90 246 211 40 48; fax: +90 246 237 11 06.
E-mail addresses: sahin@fef.sdu.edu.tr, sduosman@gmail.com (O. Sahin).

0955-2219/$ – see front matter © 2007 Elsevier Ltd. All rights reserved.
doi:10.1016/j.jeurceramsoc.2007.09.052

the load to the facet contact area of the indentation determined. This method is known as conventional indentation. One general disadvantage of this method pertains to the facet contact area measured after the load is removed. It has been argued that the area may be susceptible to elastic recovery. Secondly, at loads of a few grams the indentation dimensions are about a few micrometers and the penetration depths into the solid are about an order of magnitude smaller. It is difficult to measure such dimensions optically with a high degree of accuracy. Therefore, conventional indentation hardness obtained from microscopic observation of the indented cavity cannot give reliable mechanical properties of materials. The second method for determining the mechanical properties of solids is the depth-sensing indentation (DSI) or dynamic indentation method. This method offers great advantages over the conventional indentation test in two aspects. First, apart from hardness (or strength), the method can provide well-defined mechanical parameters such as the elastic modulus of the interfacial zone. Second, the load and depth of an indentation are continuously monitored (Fig. 1) and optical observation and measurements of the diagonal lengths of the indent/impression, which can be difficult and subjected to inaccuracy, are no longer required.[11] In this study, therefore, the mechanical properties of porous SiAlON-based ceramics prepared by pressureless sintering of the mechanically activated β-SiAlON precursor powders have been characterized by using the DSI method due to its many advantages over the conventional method.

2. Theoretical background

Two mechanical properties, namely, dynamic hardness H_d and reduced elastic modulus E_r can be obtained with the peak indentation test load and penetration depth data. Various models have been proposed by different authors to determine the aforementioned parameters.[12,13] These models are generally based on the use of load–unload curves in the dynamic indentation technique. Among these models, the Oliver–Pharr model is the one that has been frequently used in hardness test interpretation. The Oliver–Pharr data analysis procedure begins with fitting an unloading curve to an empirical power-law relation.

$$P = \alpha(h - h_f)^m \tag{1}$$

where P is the indentation test load, h the penetration depth, h_f the final unloading depth, α a geometric constant, and m is a power law exponent that is related to the geometry of the indenter. Typical m values vary from 1 to 2 depending on indenter geometry.[14] The unloading contact stiffness, S, is then established by differentiating Eq. (1) at the maximum depth of penetration, $h = h_{max}$ (i.e., Eq. (2))

$$S = \left(\frac{dP}{dh}\right)_{h=h_{max}} = \alpha m(h_{max} - h_f)^{m-1} \tag{2}$$

Then the contact depth, h_c, is calculated using the following equation

$$h_c = h_{max} - \beta\frac{P_{max}}{dP/dh} \tag{3}$$

where P_{max} is the peak indentation test load and β is a constant dependent on indenter geometry. It has been shown that β has an empirical value of 0.75 for the Vickers indenter.[15]

The hardness is usually defined as the ratio of the peak indentation test load, P_{max}, to the projected area of the hardness impression, A_c. The dynamic hardness is thus calculated from

$$H_d = \frac{P_{max}}{A_c} = \frac{P_{max}}{26.43h_c^2} \tag{4}$$

On the other hand, the peak indentation test load–penetration depth behavior can be effectively used in defining a reduced elastic modulus, E_r through the equation

$$\frac{1}{E_r} = \frac{1 - \nu_s^2}{E_s} + \frac{1 - \nu_i^2}{E_i} \tag{5}$$

where E and ν are the Young's modulus and Poisson's ratio with the subscripts s and i indicating sample and indenter, respectively. E_r, the reduced elastic modulus of a sample, is given by

$$E_r = \frac{S}{2}\frac{\sqrt{\pi}}{\sqrt{26.43}h_c} \tag{6}$$

It is clearly seen that the aforementioned computational procedure can be successfully used to calculate the H_d and E_r of SiAlON ceramic by DSI experiments.

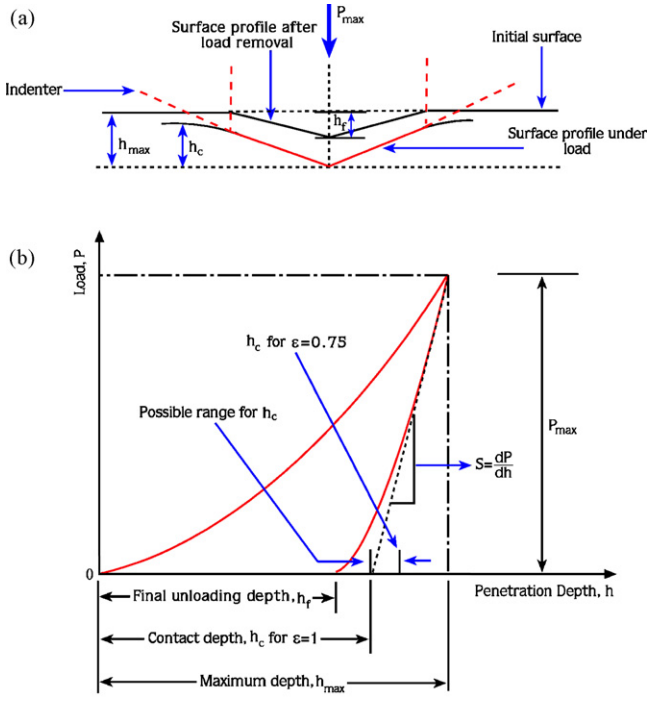

Fig. 1. Typical load-indentation depth curve generated during a depth-sensing indentation experiment, indicating key parameters needed for analysis.

3. Experimental procedure

The initial powders were α-Si_3N_4 (H.C. Starck-B7, 10–15 wt.% of β-Si_3N_4), AlN (H.C. Starck-C), and α-

Al_2O_3 prepared from $Al(OH)_3$ by firing at 1200 °C (total contaminants less than 0.2 wt.%, d_{50}-16 μm, SSA_{BET}, 0.8 $m^2\,g^{-1}$). The mixture was batched according to $z = 0.5$ in β-$Si_{6-z}Al_zO_zN_{8-z}$ solid solution (α-Si_3N_4 = 91.5 wt.%, AlN = 2.4 wt.%, Al_2O_3 = 6.1 wt.%), activated in a MPP-1 planetary mill (TTD, RU) with acceleration of the centrifugal field of 28 g, with silicon nitride balls for 45 min. The resultant powder was dispersed in an isotropic mixture of 60 vol.% methylethylketone (MEK) (Aldrich) and 40 vol.% ethanol (POCH). Three weight percent of Hypermer KD1 (Imperial Chemical Industries PLC, UK) was used as a dispersant. The suspension was mixed on the roller bench for 24 h. After drying the powders were crushed with a pestle and mortar, uniaxially cold pressed and finally cold isostatically pressed with 200 MPa. Heating in air at 600 °C for 2 h was applied in order to remove the residual polymer dispersant. Green density attained the value of 66%. The pressed tablets were contained within a powder bed of Si_3N_4/BN powder within a BN crucible with a lid. Sintering was carried out in a graphite furnace (Thermal Technology) in flowing nitrogen at temperature of 1600 °C for 60 min. The size and mass of the specimens were controlled. The density was determined by the Archimedes technique in distilled water. XRD studies were performed on the polished cross section of the tablets and Rietveld refinement method was used for calculation of the phases present. To examine the surfaces, investigations were performed by LEO Evo-40 VPX scanning electron microscope (SEM). For SEM examinations, the samples were coated with a gold thin layer to avoid charging effects.

Hardness measurements of SiAlON ceramic were performed with a dynamic ultra-microhardness tester (Shimadzu, DUH-W201S), having a maximum penetration depth 10 μm and an indenter shift resolution of 1 nm, at room temperature. A load cell and displacement-voltage dilatometer (LVDT) was used to control the applied load and to measure the penetration depth of indenter. For an easier interpretation of mechanical behavior at various depths, the maximum load was changed at regular intervals; 200–1800 mN under a loading/unloading rate of 4.4130 mN/s. For a particular load at least five indentation tests were conducted on the sample surface to increase the reliability of experimental results.

4. Results and discussion

4.1. Characterization of the resultant SiAlON-based ceramic

The resultant ceramic was a porous material (porosity, 19.9 vol.%; density, 2.47 g cm^{-3}). The final phase composition consisted of 39.4 wt.% of α-Si_3N_4, 45.4 wt.% of β-SiAlON with $z = 0.8$ and 15.2 wt.% of O'-SiAlON. Lack of eutectic liquid phase during sintering at 1600 °C effected in an incomplete conversion of α-Si_3N_4 to β-SiAlON solid solution. Presence of O'-SiAlON and a slight mass increase (0.2 wt.%) after densification showed a limited oxidation of the activated powders during reaction sintering. SEM micrographs of SiALON ceramic have been shown before (Fig. 2a) and after (Fig. 2b) the indentation tests. It was observed that the microstructure of the samples reveals nearly homogenous porosity distribution. Moreover, any additional cracks on the sample surface were not detected after the tests.

4.2. Loading–unloading data analysis

The loading–unloading curves with increasing loads of the SiAlON ceramic are given in Fig. 3. It is clearly seen that the sample exhibits elastoplastic behavior at room temperature. However, this characteristic cannot completely indicate whether the specimen has brittle or ductile properties. In the mean time, loading curves under different peak loads can be accurately fitted by one curve due to their overlapping characters. The unloading curves show the similar behavior if they are shifted according to their final depths. Therefore, it can be suggested that the SiAlON sample has similar elastic and plastic deformation mechanism for our experimental load range.

DSI values at each imposed depth, H_d, was calculated using Eq. (4). The peak indentation test load dependence of dynamic

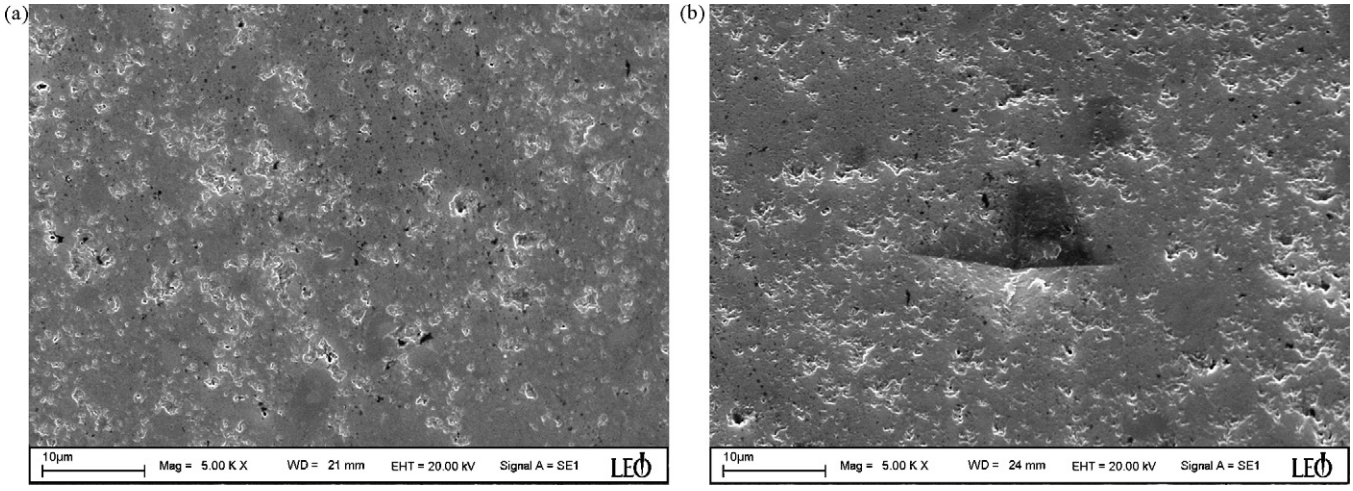

Fig. 2. (a) SEM image of SiALON ceramic before the indentation test and (b) SEM image of SiALON ceramic after the indentation test.

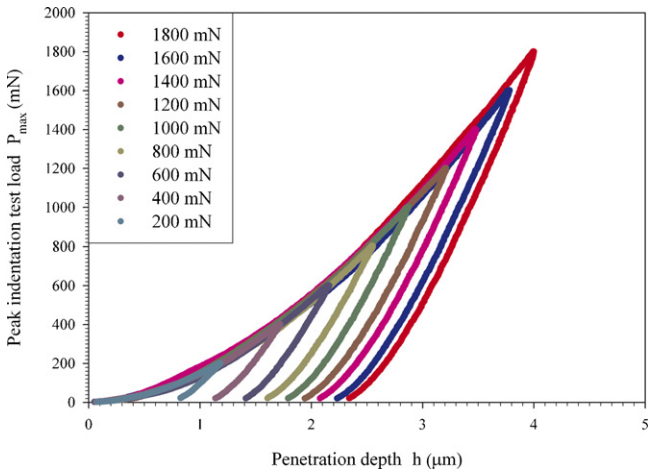

Fig. 3. Peak indentation test load–penetration depth curve of SiAlON sample at room temperature.

hardness data obtained from the examined material is shown in Fig. 4. The dynamic hardness values decrease with increasing peak indentation test load. The apparent H_d is a function of the applied load at low peak indentation test loads, where there is no constant value for the hardness (H_{LD}; load-dependent hardness). At high-peak indentation test loads, the hardness is constant with respect to the indentation test load and a single, well-defined hardness value exists (H_{LI}; load-independent hardness). H_{LI} has also been referred to as the "true" hardness in some of the literature. This behavior is called indentation size effect (ISE).[16,17]

The ISE has been examined extensively for different kind of materials. In order to describe the ISE behavior of materials, several relationships between the applied peak indentation test load, P_{max}, and the contact depth, h_c, have been proposed.[18–21] Below some selected models are first described and then applied to analyze the experimental dynamic hardness data on porous SiAlON ceramic.

4.3. Meyer's law and present data

The simplest way for describing the ISE is Meyer's law[22,23] which uses correlation technique between the peak indentation test load and the contact depth using a simple power law (Eq. (7)),

$$P_{max} = Ah_c^n \quad (7)$$

where A and n are constants derived directly from curve fitting of the experimental data. Especially, the exponent n, sometimes referred to the Meyer index, is usually considered as a measure of ISE. For the normal ISE behavior, the exponent is $n < 2$. When $n > 2$, there is the reverse ISE behavior. Compared to the definition of the apparent hardness (Eq. (7)), no ISE would be observed for $n = 2$. If hardness is load-independent ($n = 2$) modified Meyer's law called Kick's Law[24,20,21] given in Eq. (8) is used:

$$P_{max} = A_0 h_c^2 \quad (8)$$

According to the Meyer law, the indentation data for the material examined in the present study was plotted in Fig. 5. The data showed linear relationship, implying that the traditional Meyer's law was suitable for describing the indentation data. The best-fit values of the parameters A and n were 0.048, 0.541, respectively, in terms of linear regression analyses. The calculated n value pointed out higher apparent dynamic hardness values at lower loads, due to the presence of an ISE. It is generally argued that the exponent n characterizes the hardening characteristic of a material. The lower value of n, the more difficult it is to deform it. However, up to now neither the physical meaning of the Meyer index n has been understood nor the physical explanation of the interdependence between n and A has been given.[20]

4.4. Hays–Kendall approach and present data

The H_d dependence of the experimental data at peak indentation test load can be explained by Hays–Kendall approach,[25] which is a modified Kick's law.[24] Kick's law, Eq. (8), can be

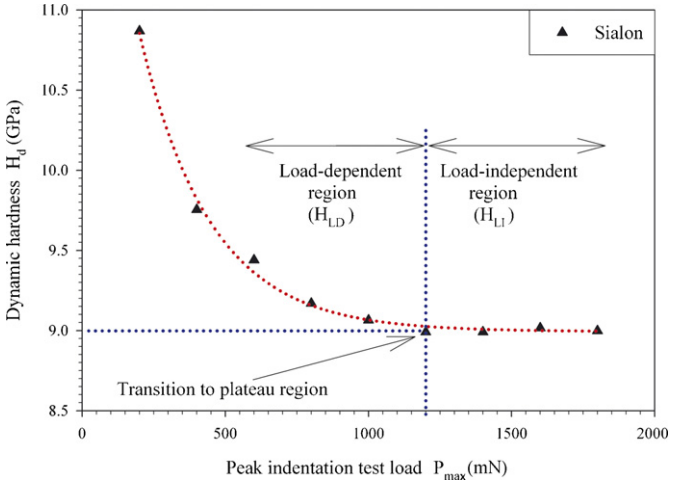

Fig. 4. Variation of the dynamic hardness with the peak indentation test load.

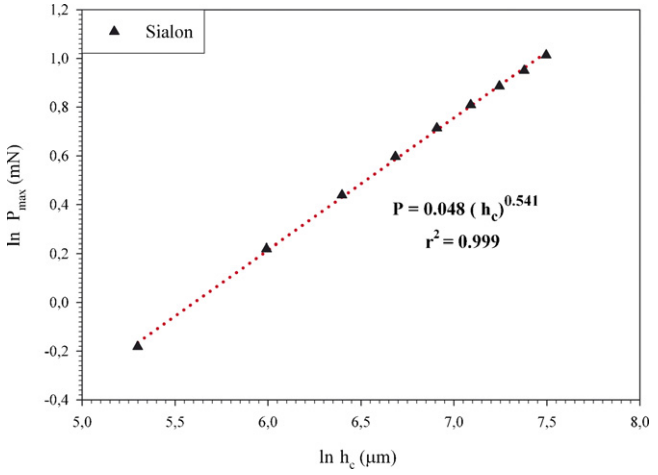

Fig. 5. Plot of ln P_{max} vs. ln h_c according to the Meyer's law.

rewritten as follow:

$$\ln [P_{\max}] = \ln A_0 + n \ln [h_c] \quad (9)$$

where A_0 is the standard hardness constant and n is the Meyer's index (or work-hardening coefficient) which is proposed to be equal to 2. Non-application of Kick's law is reflected by the observation that the slope of the graph of $\ln[P_{\max}]$ versus $\ln[h_c]$ does not come out to be 2 but is, in fact, less than 2 ($n = 0.541$). Hays and Kendall's law explains this discrepancy by assuming the following equation:

$$P_{\text{effective}} = P_{\max} - W = A_1 h_c^2 \quad (10)$$

where W is the sample resistance pressure (or Newtonian resultant pressure) and represents the minimum load that causes an indentation, A_1 is a constant, and $n = 2$ is the logarithmic index. $(P_{\max} - W)$ is an effective indentation load. Replacing $P_{\max}$ in Eq. (4) by $(P_{\max} - W)$, one gets an equation to calculate the load-independent (or true) hardness as follows:

$$H_{HK} = 0.0378 \frac{(P_{\max} - W)}{h_c^2} = 0.0378\, C_1 \quad (11)$$

From Eq. (10) a plot of $P_{\max}$ versus h_c^2 would yield a straight line where W and C_1 parameters can easily be calculated from the intersection of the curve, respectively. Such a plot for SiAlON ceramic is shown in Fig. 6. The correlation coefficient for the sample, r^2, is 0.999, implying that Eq. (10) provides a satisfactory description of the indentation data for the examined test materials. Calculated load-independent hardness value using the Hays–Kendall model, H_{HK}, is 0.163 MPa

On the other hand, Quinn and Quinn[26] have recently examined the variation of Vickers microhardness with indentation load for a variety of ceramic materials. They observed that such hardness–load curve exhibited distinct transition to a plateau of constant hardness and claimed that such curve corresponded to the intrinsic hardness value of the materials. In the present study, Fig. 4 shows the transition point (about 1200 mN) and corresponding intrinsic hardness is about 9 GPa. On the light of Quinn and Quinn[26] approximation, the load-independent hardness value calculated by Hays–Kendall model is far from the intrinsic hardness value for SiAlON sample. Therefore, it may be concluded that the Hays–Kendall model may also be insufficient to explain the ISE behavior of the present porous SiAlON sample.

4.5. Proportional specimen resistance (PSR) model and present data

Proportional specimen resistance (PSR) model is proposed by Li et al.[27] In this model, the peak indentation test load, $P_{\max}$, and the contact depth, h_c, are found to follow the relationship:

$$P_{\max} = a_1 h_c + a_2 h_c^2 \quad (12)$$

where the parameters a_1 and a_2 are constants for a given material. According to the analysis by Li and Bradt, the parameters a_1 and a_2 can be related to the elastic and the plastic properties of the test material, respectively. Especially, a_2 is suggested to be a measure of the so called "true hardness; H_{PSR}". For the indentation test with a Vickers indenter, H_{PSR} can be determined directly from a_2 with:

$$H_{PSR} = \frac{P_{\max} - a_1 h_c}{26.43 h_c^2} = \frac{a_2}{26.43} \quad (13)$$

On the other hand, Eq. (12) can be rearranged as Eq. (14) to determine both a_1 and a_2 from the plot of $P_{\max}/h_c$ against h_c:

$$\frac{P_{\max}}{h_c} = a_1 + a_2 h_c \quad (14)$$

According to the Eq. (14), a plot of $P_{\max}/h_c$ versus h_c should yield a straight line, theoretically. Fig. 7 shows such a plot where the a_1 and a_2 parameters can easily be calculated from the intersection point and slope of the curve, respectively. The best-fit a_1 and a_2 parameters and the corresponding load-independent hardness values, H_{PSR}, are -0.242 mN/μm, 4.620×10^{-3} mN/μm^2, and 0.175 MPa, respectively. Load-independent hardness value is far from the intrinsic hardness value for the SiAlON sample. Therefore, the PSR model may also be insufficient to explain

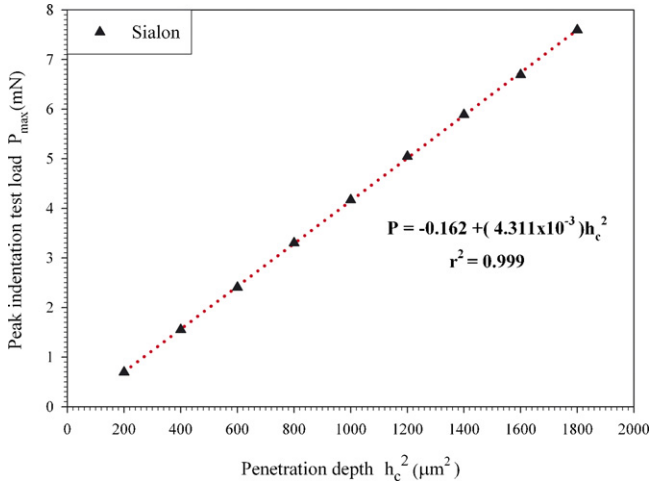

Fig. 6. Plot of $P_{\max}$ vs. h_c^2 according to the Hays–Kendall model.

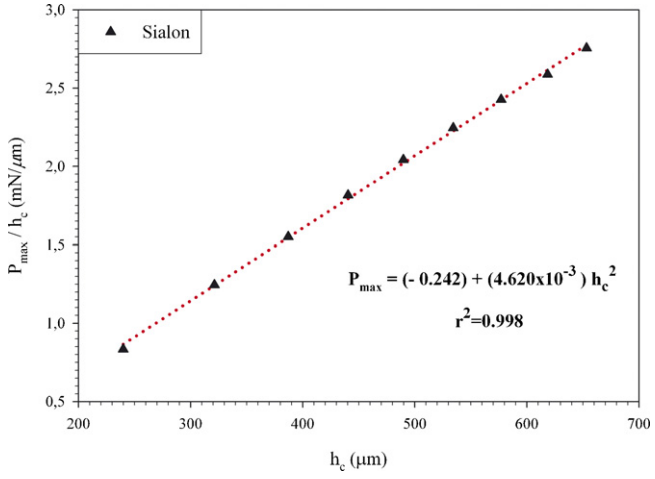

Fig. 7. Plot of $P_{\max}/h_c$ vs. h_c according to the PSR model.

the ISE behavior of the present SiAlON sample, same as the Hays–Kendall model.

4.6. Modified proportional specimen resistance (MPSR) model and present data

Recently, Modified PSR model has been proposed by Gong et al.[18] to investigate the ISE behavior in various materials. The model is given by Eq. (15):

$$P_{\max} = a_0 + a_1 h_c + a_2 h_c^2 \tag{15}$$

where a_0 is a constant related to the surface residual stresses associated with the surface machining and polishing and a_1 and a_2 are the same parameters as given in Eq. (12).

Similar to the PSR model, H_{MPSR} can be determined directly from a_2 with:

$$H_{\mathrm{MPSR}} = \frac{P_{\max} - a_0 - a_1 h_c}{26.43 h_c^2} = \frac{a_2}{26.43} \tag{16}$$

The values of a_0, a_1, and a_2 parameters may be determined by plotting the experimental $P(h)$ data as $P_{\max}$ versus h_c plot. Typical example of the plot of $P_{\max}$ versus h_c with $r^2 = 0.999$ is shown in Fig. 8. The estimated best-fit values of a_0, a_1, a_2 and H_{MPSR} values are 5.533×10^1 mN, -2.109×10^1 mN/μm, 2.376×10^2 mN/μm^2, and 8.981 GPa, respectively. The H_{MPSR} value is closer to the plateau value compared with the results of the other models. Therefore, the MPSR model, calculation of the H_{LI} value, seems to be more reasonable than the others.

The response of materials to indentation is determined by their fundamental mechanical properties, and therefore the potential exists to extract certain basic mechanical properties from hardness tests. For example, both the hardness test and the tensile test measure the resistance of a metal to plastic flow, and the results of these tests may closely parallel each other. The hardness test is preferred because it is simple, easy, and relatively nondestructive. The possibility of determination of the yield strength or the tensile strength from a simple hardness measurement is very appealing. The yield strength σ_y can be calculated from the load-independent hardness value.[28]

$$\sigma_y = \left(\frac{H_{\mathrm{LI}}}{2.9}\right)[1-(n-2)]\left\{12.5\frac{n-2}{1-(n-2)}\right\}^{n-2}, \quad \text{for Meyer's index } n > 2 \tag{17}$$

If $n \leq 2$, then this equation can be reduced to $\sigma_y = H_{\mathrm{MPSR}}/3$.[29,16] In the present case, i.e., n is not greater than 2, the equation $\sigma_y = H_{\mathrm{MPSR}}/3$ can be applied. σ_y is found as 2.993 GPa for the examined SiAlON sample.

On the other hand, reduced elastic modulus, E_r, is obtained from the analysis of the unloading curves using the Oliver and Pharr method as mentioned previously. Eq. (6) can be rearranged as follow:

$$S = \frac{dP}{dh} = \frac{2}{\sqrt{\pi}} E_r \sqrt{26.43} h_c \tag{18}$$

Eq. (18) is the basic equation for determination of reduced elastic modulus by DSI technique. The key quantities are the initial unloading contact stiffness, $S = dP/dh$ (i.e., the slope of the initial portion of the unloading curve) and the real contact depth, h_c in order to determine E_r. Using the experimentally determined S and h_c, the reduced elastic modulus by indentation was calculated and the results are shown in Fig. 9. It is found that the extracted reduced elastic modulus also exhibits a strong peak-load dependency. Therefore, it is concluded that reduced elastic modulus cannot be extracted from the peak indentation test load–penetration depth curve in terms of only one peak load.

As seen from Eq. (18), there is a linear relationship between initial unloading stiffness, S, and the contact depth at peak load, h_c. Hence, the reduced elastic modulus can be obtained directly from the slope of the best-fit lines for the SiAlON ceramic. In Fig. 10, the experimentally determined S is plotted as a function of the contact depth at peak load, h_c, obviously, a good linearity exist between these two quantities for the examined material. The correlation coefficients obtained from the linear regression analysis is 0.997.

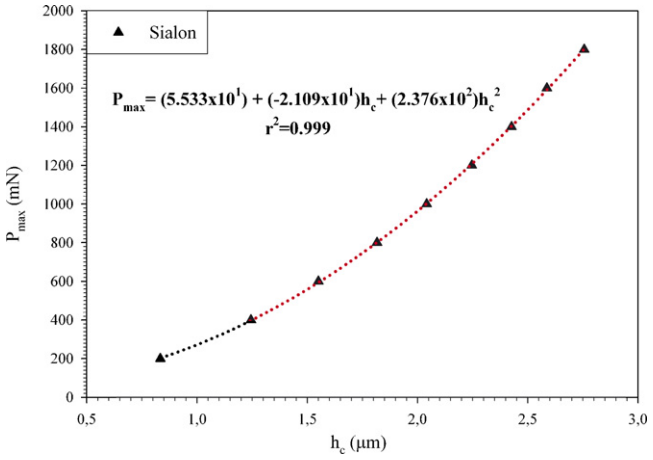

Fig. 8. Plot of $P_{\max}$ vs. h_c according to the MPSR model.

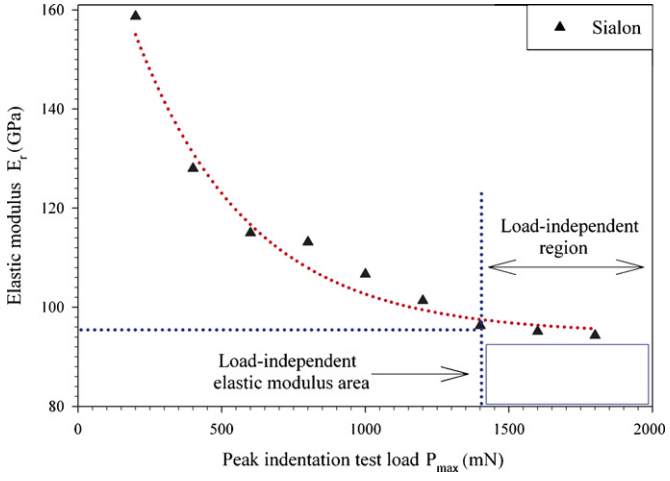

Fig. 9. Elastic modulus extracted from the analysis of the peak indentation test load penetration depth curves as a function of the peak loads for SiAlON sample.

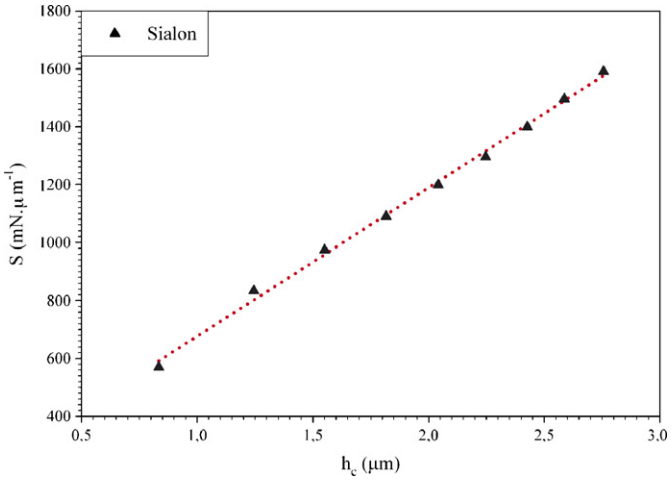

Fig. 10. Variation of the initial unloading stiffness with the contact depth at peak load for SiAlON ceramic.

The load-independent elastic modulus value obtained from the slopes of the best-fit lines in Fig. 10. Calculated E_r value is 88.3 GPa. The value is very close to the load-independent elastic modulus area shown in Fig. 9.

5. Conclusion

Depth-sensing indentation technique has been used to measure the mechanical properties of porous SiAlON-based ceramic. The dynamic hardness and reduced elastic modulus of the sample was calculated by analyzing the unloading segments of the peak indentation test load–penetration depth curves using the widely adopted Oliver and Pharr method. The results can be summarized as follows:

1. The measured dynamic indentation hardness values of porous SiAlON sample is seem to be load-dependent.
2. The variation of H_d follows the normal ISE trend, i.e., a decrease in H_d with an increase load in the low-load region beyond where becomes relatively constant. This type of variation in H_d can be explained by Meyer's relationship up to a certain value of load. However, no useful knowledge of the origin of the observed ISE is gained from this empirical equation.
3. Calculated load-independent hardness values of H_{HK} (based on the Hays–Kendal model) and H_{PSR} (based on the proportional specimen resistance model) are obviously below the plateau region. Therefore, the Hays–Kendall and PSR model does not accurately describe the ISE behavior, which observed in porous SiAlON sample.
4. Calculated load-independent hardness values by Modified PSR model are more convenient than those obtained by the other models.
5. The load-independent reduced elastic modulus, E_r, extracted directly using the conventional stiffness equation, Eq. (18), also exhibits a peak-load dependency. Therefore, a reasonable peak-load independent modulus can be determined directly from the slope of the best-fit straight line between initial unloading stiffness, S, and the contact depth at peak load, h_c. The obtained value is 88.3 GPa.

Acknowledgements

The authors would like to acknowledge the financial support (Project no.: 2003K120510) by Turkish State Planning Organization (DPT). The partially financial support by 6th FP under the project no.: ACTIVATION NMP2-CT-2004-505885 is also gratefully acknowledged.

References

1. Jack, K. H., SiAlONs and related nitrogen ceramics. *Mater. Sci.*, 1976, **11**, 1135–1158.
2. Ziegler, G., Heinrich, J. and Wötting, G., Relationships between processing, microstructure and properties of dense and reaction-bonded silicon nitride. *J. Mater. Sci.*, 1987, **22**, 3041–3086.
3. Riley, F. L., Production, properties and applications of silicon nitride ceramics. *Sprechsaal*, 1985, **118**(3), 225–233.
4. Greil, P. and Weiss, J., Evaluation of the microstructure of β-SiAlON solid solution materials containing different amounts of amorphous grain boundary phase. *J. Mater. Sci.*, 1982, **17**, 1571–1578.
5. Yang, J. F., Beppu, Y., Zhang, G. J. and Ohji, T., Corrosion behaviour of porous SiAlON ceramics. *J. Am. Ceram. Soc.*, 2002, **85**(7), 1879–1881.
6. Yang, J. F., Zhang, G. J., She, J. H., Ohji, T. and Kanzaki, S., Improvement of mechanical properties and corrosion resistance of porous β-SiAlON ceramics by low Y_2O_3 additions. *J. Am. Ceram. Soc.*, 2004, **87**(9), 1714–1719.
7. Tatli, Z. and Thompson, D. P., Low temperature densification of silicon nitride materials. *J. Eur. Ceram. Soc.*, 2007, **27**, 791–795.
8. Sopicka-Lizer, M., Tańcula, M., Pawlik, T., Kochnev, V. and Fokina, E., The new top-to-bottom method of SiAlON precursor preparation by activation in a planetary mill with a high acceleration. *Mater. Sci. Forum*, 2007, **554**, 59–64.
9. Rice, R. W., *Porosity of Ceramics*. Marcel Dekker, New York, 1998.
10. Schultz, K. and Durst, M., Advantages of an integrated system for hot gas filtration using rigid ceramic elements. *Filtr. Separat.*, 1994, **31**(1), 25–28.
11. Uzun, O., Kölemen, U., Çelebi, S. and Güçlü, N., Modulus and hardness evaluation of polycrystalline superconductors by dynamic microindentation technique. *J. Eur. Ceram. Soc.*, 2005, **25**(6), 969–977.
12. Doerner, M. F. and Nix, W. D., A method for interpreting the data depth sensing indentation instruments. *J. Mater. Res.*, 1986, **1**(4), 601–609.
13. Oliver, W. C. and Pharr, G. M., An improved technique for determining hardness and elastic modulus using load and displacement sensing indentation. *J. Mater. Res.*, 1992, **7**(6), 1564–1583.
14. Gong, J., Miao, H. and Peng, Z., A new function for the description of the nanoindentation unloading data. *Scripta Mater.*, 2003, **49**(1), 93–97.
15. Torres, F., Benino, Y., Fujiwara, T. and Komatsu, T., Evaluation of elastic/mechanical properties of some glasses and nanocrystallized glass by cube resonance and nanoindentation methods. *Mater. Res. Bull.*, 2004, **39**(10), 1431–1443.
16. Sahin, O., Uzun, O., Kolemen, U. and Uçar, N., Vickers microhardness studies of β-Sn single crystals. Materials characterization. *Mater. Charect.*, 2007, **58**, 197–204.
17. Kölemen, U., Uzun, O., Aksan, M. A., Güçlü, N. and Yakıncı, E., An analysis of load-depth data in depth-sensing microindentation experiments for intermetallic MgB_2. *J. Alloys Compd.*, 2006, **415**(1–2), 294–299.
18. Gong, J., Wu, J. and Guan, Z., Examination of the indentation size effect in low-load vickers hardness testing of ceramics. *J. Eur. Ceram. Soc.*, 1999, **19**(15), 2625–2631.
19. Gong, J., Zhao, Z., Guan, Z. and Miao, H., Load-dependence of Knoop hardness of Al_2O_3-TiC composites. *J. Eur. Ceram. Soc.*, 2000, **20**(12), 1895–1900.

20. Sangwall, K., Surowska, B. and Blaziak, P., Analysis of the indentation size effect in the microhardness measurement of some cobalt-based alloys. *Mater. Chem. Phys.*, 2002, **77**(2), 511–520.
21. Sangwall, K., Surowska, B. and Blaziak, P., Relationship between indentation size effect and material properties in the microhardness measurement of some cobalt-based alloys. *Mater. Chem. Phys.*, 2003, **80**(2), 428–437.
22. Meyer, E., Untersuchungen über Harteprufung und Harte. *Phys. Z*, 1908, 66–74.
23. Kölemen, U., Analysis of ISE in microhardness measurements of bulk MgB_2 superconductors using different models. *J. Alloys Compd.*, 2006, **425**, 429–435.
24. Kick, F., *Das Gesetz der Proportionalen Widerstände und seine Anwendung*. Felix, Leipzig, 1885 .
25. Hays, C. and Kendall, E. G., An analysis of Knoop microhardness. *Metall*, 1973, **6**(4), 275–282.
26. Quinn, J. B. and Quinn, G. D., Indentation brittleness of ceramics: a fresh approach. *J. Mater. Sci.*, 1997, **32**, 4331–4346.
27. Li, H. and Bradt, R. C., The microhardness indentation load/size effect in rutile and cassiterite single crystals. *J. Mater. Sci.*, 1993, **28**(4), 917–926.
28. Cahoon, J. P., Broughton, W. H. and Katzuk, A. R., Determination of yield strength from hardness measurements. *Metal. Trans. Metall Trans.*, 1971, **2**, 1979–1983.
29. Pal, T. and Kar, T., Vickers microhardness studies of L-arginine halide mixed crystals. *Mater. Sci. Eng. A*, 2003, **354**(1–2), 331–336.